Double-Edged Swords as Cancer Therapeutics: Novel, Orally Active, Small Molecules Simultaneously Inhibit p53–MDM2 Interaction and the NF-κB Pathway

ARTICLE *in* JOURNAL OF MEDICINAL CHEMISTRY · JANUARY 2014

Impact Factor: 5.45 · DOI: 10.1021/jm401800k · Source: PubMed

9 AUTHORS, INCLUDING:

Chunlin Zhuang
Second Military Medical University, Shanghai
24 PUBLICATIONS **155** CITATIONS
SEE PROFILE

Jianzhong Yao
Second Military Medical University, Shanghai
71 PUBLICATIONS **806** CITATIONS
SEE PROFILE

Chunquan Sheng
Second Military Medical University, Shanghai
122 PUBLICATIONS **1,200** CITATIONS
SEE PROFILE

Wannian Zhang
Second Military Medical University, Shanghai
83 PUBLICATIONS **1,151** CITATIONS
SEE PROFILE

Journal of Medicinal Chemistry

Article

pubs.acs.org/jmc

Double-Edged Swords as Cancer Therapeutics: Novel, Orally Active, Small Molecules Simultaneously Inhibit p53−MDM2 Interaction and the NF-κB Pathway

Chunlin Zhuang,[†,‡] Zhenyuan Miao,*[,†] Yuelin Wu,[†] Zizhao Guo,[†] Jin Li,[†] Jianzhong Yao,[†] Chengguo Xing,[‡] Chunquan Sheng,*[,†] and Wannian Zhang*[,†]

[†]School of Pharmacy, Second Military Medical University, 325 Guohe Road, Shanghai 200433, People's Republic of China

[‡]Department of Medicinal Chemistry, College of Pharmacy, University of Minnesota, 2231 Sixth Street SE, Minneapolis, Minnesota 55455, United States

ABSTRACT: Simultaneous inactivation of p53 and hyperactivation of nuclear factor-κB (NF-κB) is a common occurrence in human cancer. Currently, antitumor agents are being designed to selectively activate p53 or inhibit NF-κB. However, there is no concerted effort yet to deliberately design inhibitors that can simultaneously do both. This paper provided a proof-of-concept study that p53−MDM2 interaction and NF-κB pathway can be simultaneously targeted by a small-molecule inhibitor. A series of pyrrolo[3,4-*c*]pyrazole derivatives were rationally designed and synthesized as the first-in-class inhibitors of p53−MDM2 interaction and NF-κB pathway. Most of the compounds were identified to possess nanomolar p53−MDM2 inhibitory activity. Compounds **5q** and **5s** suppressed NF-κB activation through inhibition of IκBα phosphorylation and elevation of the cytoplasmic levels of p65 and phosphorylated IKKα/β. Biochemical assay for the kinases also supported the fact that pyrrolo[3,4-*c*]pyrazole compounds directly targeted the NF-κB pathway. In addition, four compounds (**5j**, **5q**, **5s**, and **5u**) effectively inhibited tumor growth in the A549 xenograft model. Further pharmacokinetic study revealed that compound **5q** exhibited excellent oral bioavailability (72.9%).

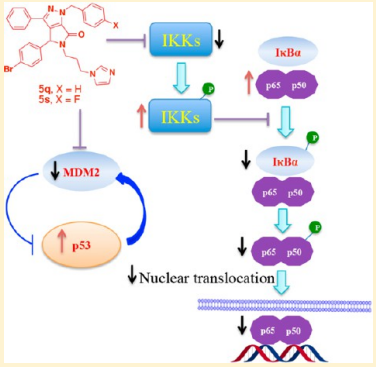

INTRODUCTION

The p53, a DNA-binding transcription factor, has been one of the most intensively studied tumor suppressors over the past 20 years.[1,2] It plays a crucial role in DNA repair, differentiation, senescence, apoptosis, and cell-cycle arrest.[1,3] Basically, its function is severely impaired by up-regulation of its key negative regulator, MDM2.[4−7] The *N*-terminal domains of MDM2 bind to the sequence (residues 15−29) in the intrinsically disordered *N*-terminus of p53.[8−10] The binding cavities within MDM2 are important targets for antitumor drug therapy that would release p53. Because of the importance of p53−MDM2 as a pharmaceutical target, several nonpeptide inhibitors have been reported in recent years.[11−14] Among them, the most potent p53−MDM2 inhibitors are the nutlins,[13] benzodiazepines,[15] spiro-oxindoles,[16,17] and piperidinones.[18] Very recently, we successfully identified novel p53−MDM2 inhibitors bearing the pyrrolidone scaffold by structure-based design.[19] These compounds (Figure 1) decreased p53−MDM2 binding more effectively than nutlin-3 and were proven to be potent in cancer cell lines and orally active in xenograft models.

NF-κB is a transcription factor discovered by Sen and Baltimore in 1986, which is located in the κ light chain of immunoglobulins in B-cells.[20] NF-κB proteins are a family of five DNA-binding proteins that are frequently hyperactive in cancer and in inflammatory diseases.[21−24] The NF-κB pathway is recognized to be the central mediator of immune responses

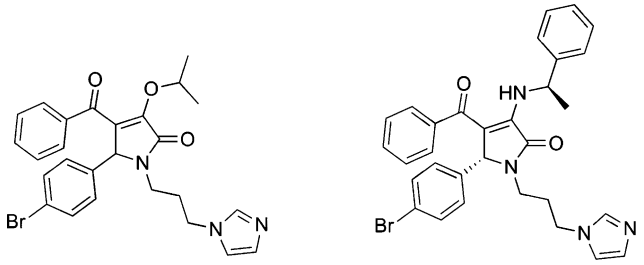

Figure 1. Representative pyrrolidone p53−MDM2 inhibitors.

in mammals.[25] More than 200 activating stimuli are known, including viruses, cytokines, stress, and bacterial and fungal products.[25] Thus, several studies have focused on the crucial reciprocal control of the p53 and the NF-κB pathways, but none has aimed to discover small molecules that simultaneously target both of these pathways.[26] Regulated cross-talk between these pathways suggested that simultaneous activation of p53 and inhibition of NF-κB would offer a synergistic effect for antitumor activity.[27] It has also been proposed that NF-κB repressed p53 stability by directly up-regulating MDM2.[28] Surprisingly, recent analysis of p53 activators has found that many of them acted as repressors of NF-κB and vice versa.[27,28]

Received: July 11, 2013
Published: January 15, 2014

   dx.doi.org/10.1021/jm401800k | *J. Med. Chem.* 2014, 57, 567−577

Scheme 1[a]

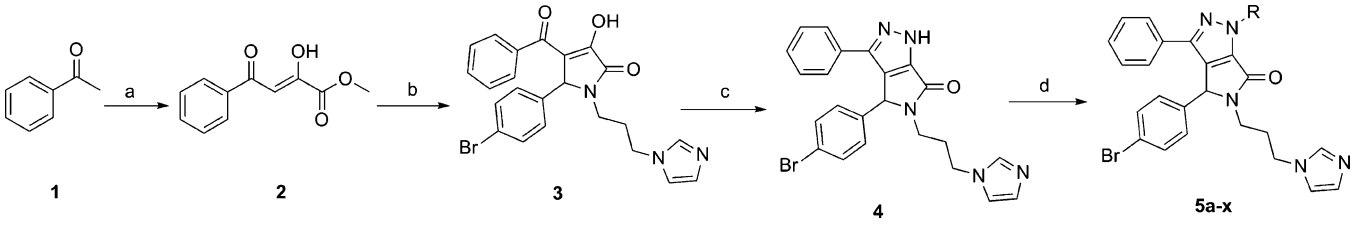

[a]Reagents and conditions: (a) ethyl oxalate, CH_3ONa/CH_3OH, reflux, 3 h; (b) 4-Br-PhCHO, *N*-(3-aminopropyl)imidazole, 1,4-dioxane, room temperature, 12 h, yield 64.5%; (c) 80% $N_2H_4{\cdot}H_2O$, CH_3COOH, 0 °C to reflux, 6 h, yield 80.6%; (d) RX, K_2CO_3, CH_3CH_2OH, reflux, 8 h, yield 23.5−75.6%.

Table 1. In Vitro Anti-Proliferative Activities of the Synthetic Compounds[a]

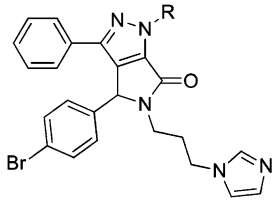

			IC$_{50}$ (μM)[c]			
compd	R	MDM2-K_i (μM)[b]	A549	NCI-H1299	U2-OS	Saos-2
4	H	47.42 ± 1.35	23.83 ± 5.15	25.68 ± 1.77	24.38 ± 0.72	26.91 ± 0.23
5a	methyl	0.17 ± 0.03	20.31 ± 0.59	20.69 ± 0.71	32.71 ± 8.15	17.49 ± 0.82
5b	ethyl	56.5 ± 10.0	5.97 ± 1.15	8.03 ± 1.86	20.49 ± 1.81	6.26 ± 0.62
5c	propyl	13.24 ± 3.40	15.98 ± 0.52	21.94 ± 1.42	20.59 ± 6.58	22.67 ± 0.17
5d	isopropyl	0.11 ± 0.025	28.84 ± 0.50	25.24 ± 3.64	34.01 ± 0.45	25.32 ± 0.20
5e	butyl	>100	21.12 ± 2.88	20.79 ± 0.27	22.82 ± 1.39	18.64 ± 0.22
5f	isobutyl	16.02 ± 1.16	22.68 ± 0.31	20.25 ± 2.69	27.67 ± 0.82	18.45 ± 3.68
5g	*tert*-butyl	2.48 ± 0.52	16.92 ± 3.29	4.52 ± 1.47	7.91 ± 1.02	2.28 ± 0.18
5h	allyl	3.82 ± 0.01	>100	>100	>100	>100
5i	propargyl	6.78 ± 1.41	25.39 ± 0.59	68.82 ± 22.04	39.43 ± 0.86	29.91 ± 1.37
5j	pentyl	0.056 ± 0.002	4.91 ± 0.11	2.92 ± 0.13	5.72 ± 0.13	2.49 ± 0.15
5k	hexyl	>100	26.98 ± 2.05	>100	>100	>100
5l	heptyl	10.8 ± 0.10	>100	>100	>100	>100
5m	octyl	>100	>100	>100	>100	>100
5n	cyclobutyl	0.23 ± 0.02	32.88 ± 2.16	32.03 ± 0.36	35.43 ± 2.88	54.18 ± 1.92
5o	cyclopentyl	0.66 ± 0.01	26.17 ± 0.89	30.27 ± 1.39	37.15 ± 1.99	31.03 ± 6.01
5p	cyclohexyl	>100	21.17 ± 2.56	27.32 ± 0.94	28.28 ± 0.31	28.96 ± 1.52
5q	benzyl	0.25 ± 0.09	36.87 ± 1.02	33.42 ± 2.60	36.78 ± 0.47	33.19 ± 0.24
5r	2-fluorobenzyl	2.51 ± 0.02	9.89 ± 1.76	5.57 ± 0.14	3.39 ± 0.20	3.60 ± 0.29
5s	4-fluorobenzyl	0.083 ± 0.003	5.82 ± 0.04	2.39 ± 0.19	2.09 ± 0.02	5.08 ± 0.55
5t	-$(CH_2)_2$OTHP	1.90 ± 0.01	18.43 ± 0.48	20.37 ± 1.65	17.63 ± 1.84	20.05 ± 0.65
5u	2-hydroxyethyl	0.28 ± 0.02	20.81 ± 1.01	19.74 ± 4.78	25.22 ± 2.64	22.71 ± 0.66
5v	$-CH_2COOCH_2CH_3$	0.96 ± 0.01	>100	>100	>100	>100
5w	$-(CH_2)_2COOCH_2CH_3$	0.72 ± 0.01	>100	88.96 ± 6.79	>100	87 ± 25
5x	$-(CH_2)_3COOCH_2CH_3$	>100	36.87 ± 0.38	23.92 ± 3.35	31.97 ± 1.10	31.35 ± 1.11
nutlin-3	–	0.093 ± 0.01	20.79 ± 1.43	16.34 ± 5.59	12.76 ± 2.42	4.14 ± 0.10

[a]All the experiments were duplicated. Data are presented as the mean ± SD. [b]Values were determined by a fluorescence polarization assay. [c]Values were measured with the MTT method.

Furthermore, there is now increasing evidence that one drug simultaneously targeting different pathways is a better approach for cancer therapy.[29] Herein, we report first-in-class small-molecule inhibitors targeting the p53−MDM2 interaction and NF-κB pathway simultaneously, which provides a novel strategy for cancer therapy. These dual-targeting inhibitors were designed on the basis of our previously identified pyrrolidone p53−MDM2 inhibitors.[19] Their modes of action were supported by a series of biochemical and cell-based assays. Several compounds also showed potent in vitro and in vivo antitumor activities, which represent promising leads for the discovery of novel antitumor agents.

RESULTS AND DISCUSSION

Chemistry. Compound **3** was prepared according to the procedures from our previous work through a two-step procedure (Scheme 1).[19] Then, it was condensed with excessive hydrazine to afford compound **4** with a new pyrrolo[3,4-

dx.doi.org/10.1021/jm401800k | J. Med. Chem. 2014, 57, 567−577

c]pyrazole scaffold. The target compounds (**5a**−**x**) were obtained by introducing aromatic, aliphatic, and polar groups on compound **4** using well-established conditions for substitution reaction.

Design Rationale. On the basis of our previously identified pyrrolidone p53−MDM2 inhibitors,[19] the dual-targeting inhibitors were designed for the following reasons: (1) compounds with the pyrrolo[3,4-*c*]pyrazole system have recently attracted significant attention because of their unique structure and broad biological activities[30−36] and (2) compounds with the pyrazole scaffold, such as celecoxib, have been identified to possess NF-κB inhibitory activity.[37−40]

p53−MDM2 Inhibitory Activity. As compared with the lead compound **3** (K_i = 0.29 μM), the fluorescence polarization assay revealed that the pyrrolo[3,4-*c*]pyrazole derivative **4** possessed a poor K_i value of 47.42 μM (Table 1). However, this compound showed significantly better solubility than the lead compound in DMSO. Thus, compound **4** was further optimized by introducing various substitutions on its pyrazole NH group. To our delight, most of the derivatives with aliphatic substituents showed increased binding activity. In particular, five of them (compounds **5a**, **5d**, **5j**, **5n**, and **5o**) exhibited potent binding activity to MDM2 with K_i values lower than 1 μM (Table 1). Among them, the methyl derivative **5a** (K_i = 0.17 μM), the isopropyl derivative **5d** (K_i = 0.11 μM), and the pentyl derivative **5j** (K_i = 0.056 μM) showed excellent inhibitory activity comparable to the drug control nutlin-3 (K_i = 0.093 μM). Structure−activity relationship (SAR) analysis demonstrated that compounds with *tert*-butyl (compound **5g**), allyl (compound **5h**), and propargyl (compound **5i**) groups on the pyrazole scaffold demonstrated moderate inhibition with K_i values ranging from 2.48 to 6.78 μM. Interestingly, the compounds with iso-aliphatic (compounds **5d** and **5f**) or tert-aliphatic (compound **5g**) groups possessed better activity than the compounds with the linear alkyl groups (compounds **5c** and **5e**). However, decreased inhibitory activity was observed for the ethyl derivative **5b** (K_i = 56.5 μM). The butyl derivative **5e** and the hexyl derivative **5k** were totally inactive. For the compounds with cycloalkane substitutions, the cyclobutyl (**5n**) and cyclopentyl (**5o**) derivatives were proven to possess potent inhibitory activity compared with the lead compound **4**. In contrast, introducing the cyclohexyl group (**5p**) resulted in the loss of the activity.

Encouraged by the above results, aromatic (compounds **5q**, **5r**, and **5s**), ester (compounds **5v**, **5w**, and **5x**), and hydroxyl (compounds **5t** and **5u**) groups were then introduced on the pyrazole scaffold. Fortunately, most of them showed significantly better activity than compound **4**. For the aromatic-substituted derivatives, the binding inhibition of the benzyl derivative **5q** (K_i = 0.25 μM) was more than 180-fold higher than that of compound **4**. Moreover, introducing a fluorine atom on position 2 or 4 of the benzyl group resulted in different inhibition of p53−MDM2 interaction. The 4-fluorobenzyl derivative **5s** had a K_i value of 0.083 μM, which was slightly more potent than the positive control, nutlin-3. In contrast, the activity of the 2-fluorobenzyl derivative **5r** was decreased by 30-fold. The introduction of the hydroxyethyl group on the pyrazole ring also had positive effects on the MDM2 inhibitory activity. Compound **5u** with free hydroxyl showed 6.7 times higher binding activity than the tetrahydropyranyl (THP)-protected compound **5t**. When the hydroxyl group of compound **5u** was replaced by ester groups, the p53−MDM2 inhibitory activity was slightly decreased for compounds **5v** and **5w**. However, the activity of the butyrate derivative **5x** was totally lost.

In Vitro Antiproliferative Activity. To investigate the in vitro antiproliferative activity of the p53−MDM2 inhibitors, four human tumor cell lines, namely, U-2 OS (wild-type p53), A549 (wild-type p53), Saos-2 (p53 null), and NCI-H1299 (p53 null), were chosen for assaying. Nutlin-3 was used as a reference compound. The obtained IC_{50} values for the p53−MDM2 inhibitors are summarized in Table 1. In general, these p53−MDM2 inhibitors displayed moderate to good activity against cancer cell lines with wild-type p53. Comparing with the totally inactive compound **3**,[19] most of the target compounds showed improved antiproliferative activities, highlighting the importance of the pyrrolo[3,4-*c*]pyrazole scaffold for the antitumor activity. Notably, compounds **5a**, **5b**, **5c**, **5g**, **5j**, **5r**, **5s**, and **5t** showed better activity against the A549 cell line than nutlin-3 (IC_{50} = 20.79 μM). Compounds **5g**, **5j**, **5r**, **5s**, and **5t** were also more active against the U-2 OS cell line than nutlin-3 (IC_{50} = 12.76 μM). Moreover, the most active p53−MDM2 inhibitors **5j** and **5s** also revealed the best inhibitory effect against A549 cell line with IC_{50} values of 4.91 and 5.82 μM, respectively. Meanwhile, these two compounds possessed potent antiproliferative activity against the U-2 OS cell line, being 2−6-fold higher than that of nutlin-3. Nevertheless, these compounds had poor selectivity over cancer cell lines with deleted p53, which inspired us to carry out further mechanistic and in vivo studies.

Western Blotting Assay for the p53 Pathway. To further validate the mechanism of MDM2 binding for compound **5s**, Western blotting was used for analyzing the levels of p53 and MDM2 proteins in A549 cancer cells. Consistent with the result of the fluorescence polarization assay, compound **5s** caused a significant dose-dependent increase in the levels of p53 and a decrease of MDM2 protein after 4 h treatment (Figure 2; all the gels were from the same experiment), mechanistically supporting the pyrrolo[3,4-*c*]-pyrazole derivatives disrupting the protein−protein interaction of p53 and MDM2.

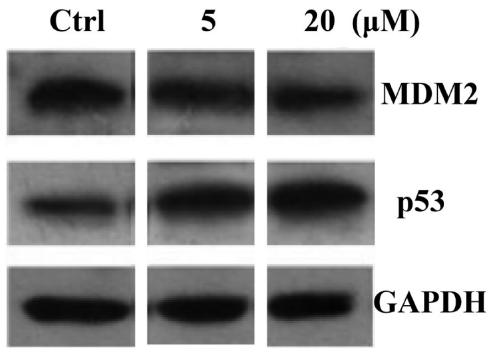

Figure 2. Cellular activity of compound **5s** for the p53 pathway activation detected by Western blotting assay (A549 cells, 4 h treatment).

Dose-Dependent and Time-Dependent Reduction Effect of Pyrrolo[3,4-*c*]pyrazole Derivatives on the NF-κB Pathway. On the basis of the cross-linking with the p53 pathway and compound design strategy mentioned above, potential inhibition of the NF-κB activation was tested. Inhibition of the NF-κB was expected to suppress the NF-κB protein translocation to the nucleus. Moreover, phosphor-

dx.doi.org/10.1021/jm401800k | J. Med. Chem. 2014, 57, 567−577

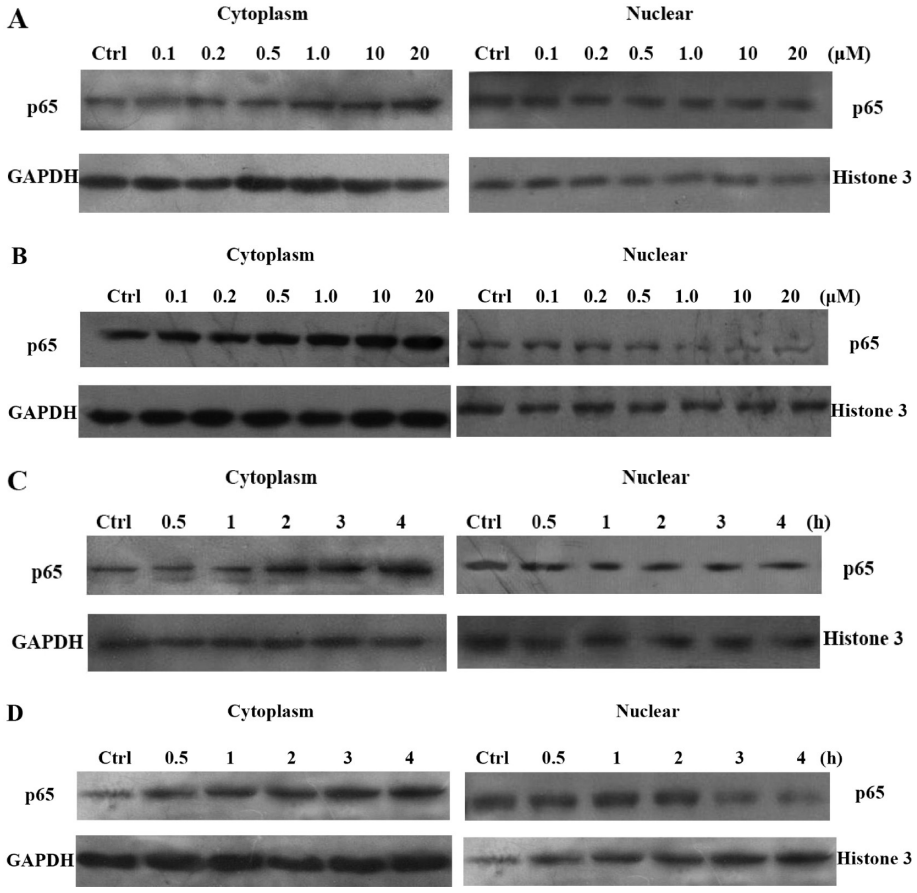

Figure 3. Cellular activity of compounds **5q** and **5s** on the NF-κB pathway detected by Western blotting assay (A549 cells): (A) dose-dependent manner for compound **5q** (4 h treatment), (B) dose-dependent manner for compound **5s** (4 h treatment), (C) time-dependent manner for compound **5q** at 10 μM, and (D) time-dependent manner for compound **5s** at 10 μM.

ylation of IκBα and IκBα kinases (IKKs) is known to be involved in the process of the activation of NF-κB.[41] To determine the effect of the highly potent compounds **5q** and **5s** on the NF-κB pathway, the relative cytoplasmic levels of p65 and IκBα and the nuclear level of p65 protein were examined by Western blotting assay. As shown in Figure 3A,B, consistent with expectations, compounds **5q** and **5s** caused dose-dependent increases in the levels of p65 in cytoplasm of A549 cells on lysis following 4 h treatment. Meanwhile, a dose-dependent decrease of these two compounds in the levels of nuclear p65 was also observed. Encouraged by these results, time-dependent examinations were performed and the p65 level of compound **5s** greatly increased at the 0.5 h time point, while the p65 level of compound **5q** changed starting from 2 h treatment (Figure 3C,D). For compound **5s**, phosphorylated IκBα was significantly inhibited in a concentration-dependent manner and the IκBα protein was observed to be slightly suppressed (Figure 4). Phosphorylation of specific serine residues of IκB proteins by IKKs targets IκB for proteasome-mediated degradation.[41] Therefore, the IKKs levels in the cytoplasm were tested to determine the potential targets of compound **5s**. It should be noted that IKKβ could not be distinguished from IKKα in this analysis with antibodies that detect both phosphorylated IKKα at Ser176/180 and IKKβ at Ser177/181. As depicted in Figure 4, incubation of the cells with compound **5s** for 4 h markedly activated the phosphorylation of IKKβ only or both IKKβ and IKKα in a dose-dependent manner, but no obvious effect was observed in

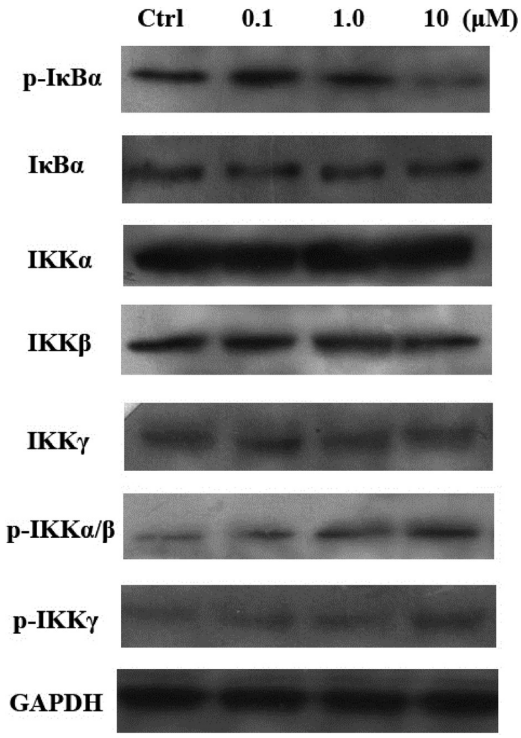

Figure 4. The effects of compound **5s** on IκBα and IκBα kinases (IKKs) detected by Western blotting assay (A549 cells, 4 h treatment).

dx.doi.org/10.1021/jm401800k | J. Med. Chem. 2014, 57, 567−577

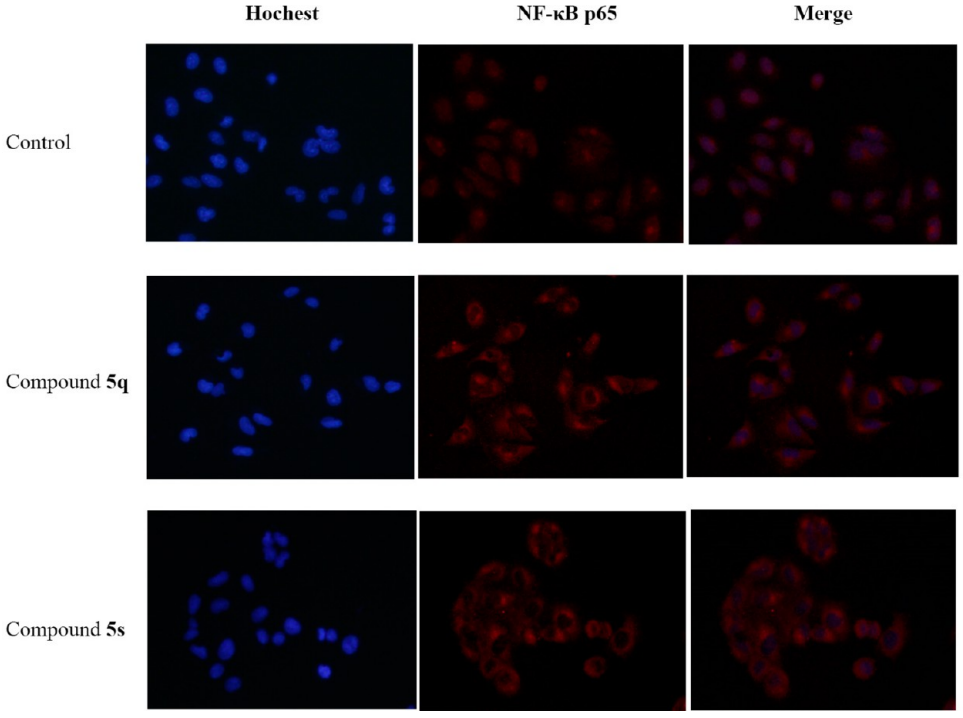

Figure 5. The effects of compounds **5q** and **5s** (10 μM) on the nuclear translocation of the p65 protein.

Table 2. Inhibitory Activities of Compound 5s against Seven Kinases of the NF-κB Pathway

IC_{50} (μM)						
IKKα	IKKβ	IKKε	CHK1[a]	Akt1[a]	Akt2	Akt3
51.8 ± 0.2	80.5 ± 1.1	78.2 ± 0.3	57.1 ± 0.1%	38.1 ± 3.8%	>100	>100

[a]Percentage of inhibition at 100 μM.

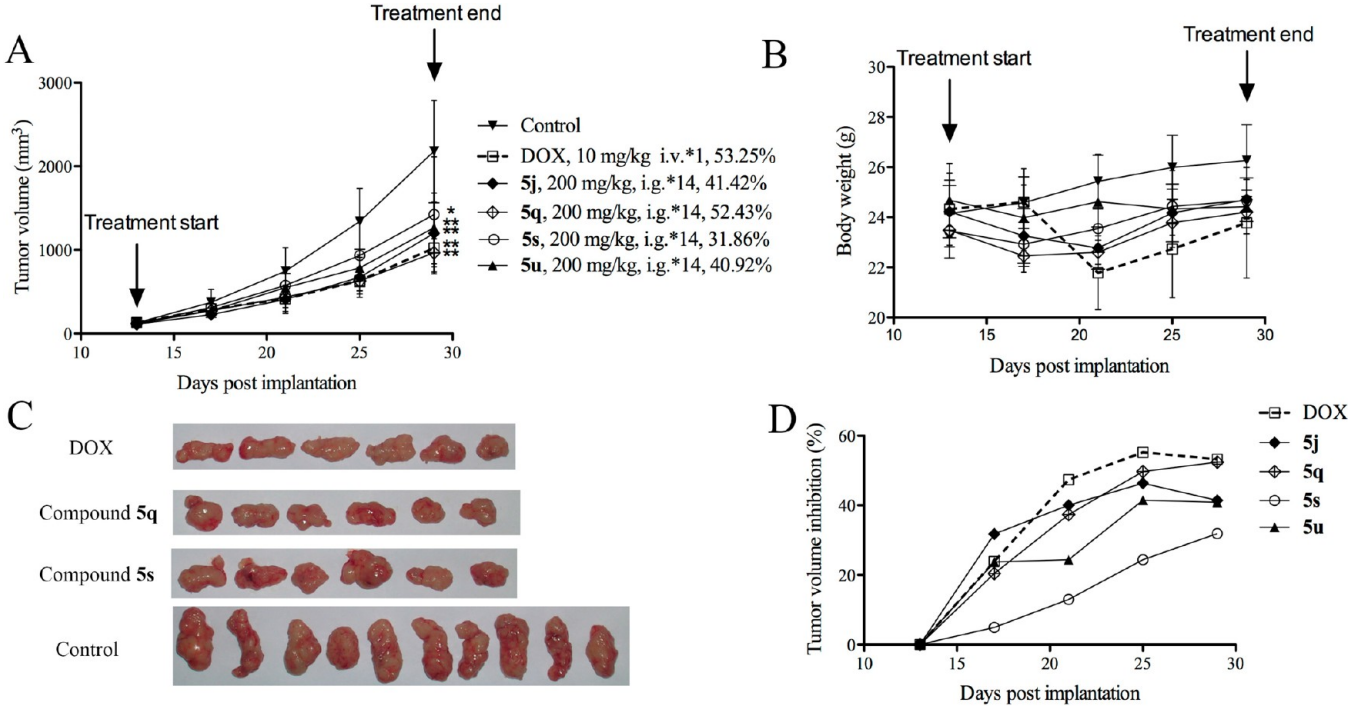

Figure 6. Inhibition of tumor growth for compounds **5j**, **5q**, **5s**, and **5u** (200 mg/kg, administered intragastrically, 14 days) against A549 xenografts in nude mice: (A) tumor volume (TV = $^1/_2ab^2$); (B) animal body weight. (C) Pictures of the tumors after treating with compounds **5q** and **5s**. (D) Variation trends of tumor volume inhibition ($1 - RTV_{tumor}/RTV_{control} \times 100\%$) for compounds **5j**, **5q**, **5s**, and **5u**. Data are presented as the mean ± SEM; $n = 6$ nude mice per group: $^*p < 0.05$, $^{**}p < 0.01$, versus control group ($n = 10$ nude mice), determined with Student's t test.

dx.doi.org/10.1021/jm401800k | J. Med. Chem. 2014, 57, 567−577

Table 3. Pharmacokinetic Parameters of Compound 5q in Sprague−Dawley Rats[a]

route	dose (mg/kg)	C_{max} (ng/mL)	$AUC_{0\text{-}t}$ (μg·h/L)	$AUC_{0\text{-}\infty}$ (g·h/L)	$MRT_{0\text{-}\infty}$ (h)	$T_{1/2}$ (h)	T_{max} (h)	CL (L/h/kg)	V_Z (L/kg)	F_{ab} (%)
i.v.	5.0	2548	1581	1589	1.21	2.11		3.18	9.74	
i.g.	100	4589	23155	23161	4.99	1.80	3.25			72.9

[a] C_{max}, maximum concentration of the compound detected in plasma; AUC, area under the curve; MRT, mean residence time; $T_{1/2}$, terminal half-life; T_{max}, peak time; CL, apparent total body clearance of the drug from plasma; V_Z, apparent volume of distribution during terminal phase; F_{ab}, absoluteoral bioavailability.

phosphorylated IKKγ and total IKK proteins, indicating that the pyrrolo[3,4-c]pyrazole derivatives suppressed NF-κB activation mainly through inhibition of IκBα phosphorylation mediated by the IKKα/β phosphorylation.

Pyrrolidone Derivatives Inhibit NF-κB Translocation to Nucleus. An indirect immunofluorescence assay was performed to analyze the NF-κB p65 nuclear translocation. As shown in Figure 5, in untreated cells (control), an intense nuclear fluorescence was observed, showing the nuclear translocation of NF-κB. Treatment with compounds **5q** and **5s** for 4 h at a dosage of 10 μM clearly diminished the intracellular p65 translocation into the nucleus from the cytoplasm of cells.

Pyrrolidone Derivative Inhibits the Kinases of NF-kB Pathways. As the inhibition of the translocation of NF-κB from the cytoplasm to the nucleus could occur with other MDM2 inhibitors, a cell-free kinase assay was then carried out to confirm whether the pyrrolo[3,4-c]pyrazole inhibitor directly targeted this pathway. Inhibition of seven related kinases was then assayed (Table 2). Compound **5s** exhibited about 100% inhibition of IKKα, -β, and -ε at a concentration of 100 μM. Particularly, **5s** inhibited IKKα with an IC_{50} value of 51.8 ± 0.2 μM. For CHK1 and Akt1, it only showed 57.1% and 38.1% inhibition at 100 μM, respectively. Moreover, no obvious effect was observed on the other two kinases, Akt2 and Akt3. Thus, the above biochemical results well supported the fact that pyrrolo[3,4-c]pyrazole compounds targeted the NF-κB by inhibiting IKKs directly rather than transcription of the p53−MDM2 inhibition.

In Vivo Antitumor Potency. To investigate the in vivo effects of the pyrrolo[3,4-c]pyrazole derivatives on tumor growth, a xenograft model was prepared by inoculating nude mice with human lung cancer A549 cells. Considering that the in vivo antitumor potency usually does not correlate well with in vitro antiproliferative activities, representative derivatives were selected according to their chemical structures and antitumor activity to evaluate their potency in xenograft models. Considering the limited aqueous solubility of our compounds, the intragastrical (i.g.) route, which is a common administration method for the p53−MDM2 inhibitors in preclinical trails and an easy method for oral administration, was selected for this in vivo study. Compounds **5j**, **5q**, **5s**, and **5u** were tested in A549 xenograft model at the dose of 200 mg/kg. As depicted in Figure 6A, i.g. administration of these four compounds for 14 days significantly inhibited tumor growth ($p < 0.05$). They produced tumor volume inhibition of 41.42%, 52.43%, 31.86%, and 40.92%, respectively (Figure 6A,D). Meanwhile, all the compounds were found to be well-tolerated during the test and instigated no significant loss of the body weight (Figure 6B), suggesting that their toxicity is low. Notably, compound **5q** showed significant tumor volume inhibition compared with doxorubicin (DOX) (53.25%) (Figure 6A,C). For compound **5s**, 31.86% of tumor volume inhibition was achieved and its tumor volume inhibition value was enhanced at every monitoring day (Figure 6D). A long-term treatment is ongoing now.

Pharmacokinetic Study of Compound 5q. Compound **5q** was selected for pharmacokinetic evaluation in rats because itshowed the best in vivo efficacy in the A549 xenograft model. Compound **5q** was administered intravenously at 5 mg/kg and intragastrically at 100 mg/kg to secure a sufficient exposure in the animal. As shown in Table 3, compound **5q** showed a relatively short half-life, approximately 2 h, for the two different administration routes, but with an adequate systemic exposure (AUC). Compound **5q** at 100 mg/kg by gavage achieved a C_{max} of 4589 ng/mL (8.31 μM) at 3.25 h (Figure 7) and $AUC_{0\text{-}\infty}$ of 23 161 μg·h/L (Table 3). To our delight, compound **5q** exhibited excellent oral bioavailability (F_{ab} = 72.9%).

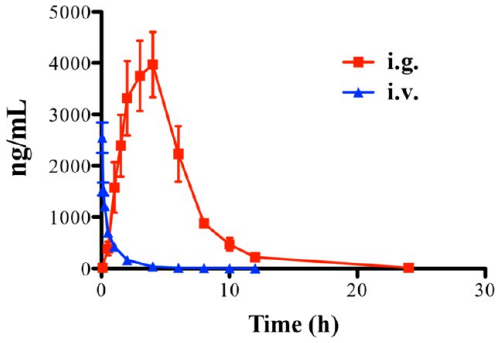

Figure 7. Plasma concentrations of compound **5q** with two administration routes in Sprague−Dawley rats.

CONCLUSION

The present investigation provided a proof-of-concept study that p53−MDM2 interaction and the NF-κB pathway can be simultaneously targeted by a small-molecule inhibitor. A series of small molecules bearing a novel pyrrolo[3,4-c]pyrazole scaffold were rationally designed and synthesized and showed potent in vitro and in vivo antitumor activities. Interestingly, compounds **5q** and **5s** were potent inhibitors, simultaneously targeting the p53−MDM2 interaction and NF-κB pathway. Further biological studies characterized the mechanism of compound **5s**. It was involved in two pathways: (1) compound **5s** directly inhibited the p53−MDM2 protein−protein interaction and (2) compound **5s** suppressed NF-κB activation mainly through inhibition of IκBα phosphorylation mediated by the IKKs phosphorylation. Biochemical assay for the kinases supported that the pyrrolo[3,4-c]pyrazole compounds directly targeted the NF-κB pathway by inhibiting IKKs. Notably, compounds **5j**, **5q**, **5s**, and **5u** were orally active and able to effectively inhibit tumor growth with low toxicity in the A549 xenograft model. Further pharmacokinetic study for compound **5q** revealed that it exhibited excellent oral bioavailability (72.9%). Further optimization studies are ongoing to identify more potent inhibitors of these two pathways.

dx.doi.org/10.1021/jm401800k | J. Med. Chem. 2014, 57, 567−577

EXPERIMENTAL SECTION

Chemistry. *General Methods.* All starting materials were commercially available and analytical pure. Melting points were measured on an uncorrected X-5 digital melting point apparatus (Gongyi City Yuhua Instrument Co., Ltd.). ^{1}H NMR and ^{13}C NMR spectra were recorded on a BRUKER AVANCE 300 spectrometer, a BRUKER AVANCE 500 spectrometer, or a BRUKER AVANCE 600 spectrometer (Bruker Co.), using TMS as an internal standard and $CDCl_3$ or DMSO-d_6 as solvents. Chemical shifts (δ values) and coupling constants (J values) are given in ppm and hertz, respectively. TLC analysis was carried out on silica gel plates GF254 (Qindao Haiyang Chemical). Flash column chromatography was carried out on silica gel 300−400 mesh using a Biotage instrument. Anhydrous solvent and reagents were all analytically pure and dried through routine protocols. The purity of the final compounds was determined using CH_3CN/H_2O (85:15) as the mobile phase with a flow rate of 1.0 mL/min on a C_{18} column.

Synthesis of Compound ***2***. A solution of diethyl oxalate (12.0 mmol) and acetophenone (**1**, 6.0 mmol) in methanol (10 mL) was added dropwise to a freshly prepared solution of CH_3ONa in CH_3OH (2.6 mL of 25% w/v, 12.0 mmol), and then the reaction was allowed to proceed under reflux for another 3 h. After cooling to room temperature, the reaction mixture was poured into water (40 mL) for 1 h, acidified with HCl (1 mL, 37% w/v) to reach pH 3−4, and extracted with diethyl ether (100 mL × 3). The combined organic extracts were washed with brine (30 mL), dried over Na_2SO_4, and filtered, and the solvent was removed in vacuum to afford the crude product **2**, which was directly used in the next step.

Synthesis of Compound ***3***. Bromobenzaldehyde (10 mmol) and *N*-(3-aminopropyl)imidazole (10 mmol) were mixed in 1,4-dioxane (10 mL). After stirring for 15 min, a solution of compound **2** (10 mmol) in 1,4-dioxane (5 mL) was dropped slowly into the solvent. Then, the mixture was stirred for another 12 h. The resulting precipitate was filtered off and recrystallized from CH_3OH to give compound **3**. Yield: 64.5%, white solid. Mp: 228−231 °C. ^{1}H NMR (300 MHz, DMSO-d_6) δ: 8.20 (s, 1H), 7.70 (d, 2H, J = 6.9 Hz), 7.46 (m, 3H), 7.36 (m, 3H), 7.30 (m, 2H), 7.15 (s, 1H), 5.46 (s, 1H), 3.95 (m, 2H), 3.51 (m, 1H), 2.61 (m, 1H), 1.83 (m, 2H). ESI-MS (m/z): 468.92 $[M + 1]^+$.

Synthesis of Compound ***4***. Compound **3** (1 mmol) and hydrazine hydrate (5 mmol) were mixed in acetic acid (10 mL) at 0 °C, stirred for 15 min, and then heated under reflux for 6 h. After completion of reaction, the solution mixture was washed with water and then extracted with CH_2Cl_2. The organic layer was then washed with water and 2% $NaHCO_3$, separated, dried (Na_2SO_4), and evaporated to dryness. The residue was purified by flash column chromatography (CH_2Cl_2:CH_3OH = 100:1) to give compound **4**. Yield: 80.6%. ^{1}H NMR (300 MHz, DMSO-d_6) δ: 14.04 (s, 1H), 7.62 (s, 1H), 7.47−7.53 (m, 4H), 7.21−7.36 (m, 5H), 7.15 (s, 1H), 6.87 (s, 1H), 6.02 (s, 1H), 3.95 (m, 2H), 3.58 (m, 1H), 2.66 (m, 1H), 1.88 (m, 2H). ESI-MS (m/z): 462.31 $[M + 1]^+$.

General Prodedure for the Synthesis of Compounds ***5a−x***. Compound **4** (1 mmol), haloalkane (2 mmol), and potassium carbonate (2 mmol) were mixed in ethanol (10 mL) and stirred under reflux for 8 h. The resulting precipitate was filtered off and the filtrate was then evaporated to dryness. The residue was purified by flash column chromatography (CH_2Cl_2:CH_3OH = 100:2) to give compounds **5a−x** in 23.5−75.6% yield.

5-(3-(1H-Imidazol-1-yl)propyl)-4-(4-bromophenyl)-1-methyl-3-phenyl-4,5-dihydropyrrolo[3,4-c]pyrazol-6(1H)-one ***(5a)***. Yield: 75.6%, light yellow solid. Mp: 155−157 °C. ^{1}H NMR (500 MHz, DMSO-d_6) δ: 7.60 (s, 1H), 7.52 (d, 2H, J = 8.3 Hz), 7.48 (d, 2H, J = 7.4 Hz), 7.21−7.30 (m, 5H), 7.15 (s, 1H), 6.87 (s, 1H), 5.99 (s, 1H), 4.05 (s, 1H), 3.96 (m, 2H), 3.58 (m, 1H), 2.65 (m, 1H), 1.89 (m, 2H). ESI-MS (m/z): 476.95 $[M + H]^+$. HPLC purity: 95.3%.

5-(3-(1H-imidazol-1-yl)propyl)-4-(4-bromophenyl)-1-ethyl-3-phenyl-4,5-dihydropyrrolo[3,4-c]pyrazol-6(1H)-one ***(5b)***. Yield: 65.3%, light yellow solid. Mp: 50−52 °C. ^{1}H NMR (300 MHz, DMSO-d_6) δ: 7.61 (s, 1H), 7.48−7.54 (m, 4H), 7.23−7.31 (m, 5H), 7.15 (s, 1H), 6.87 (s, 1H), 6.00 (s, 1H), 4.43 (t, 2H, J = 7.2 Hz), 3.97 (m, 2H), 3.57 (m, 1H), 2.67 (m, 1H), 1.90 (m, 2H), 1.55 (t, 3H, J = 7.2 Hz). ESI-MS (m/z): 490.33 $[M + H]^+$. HPLC purity: 96.5%.

5-(3-(1H-Imidazol-1-yl)propyl)-4-(4-bromophenyl)-3-phenyl-1-propyl-4,5-dihydropyrrolo[3,4-c]pyrazol-6(1H)-one ***(5c)***. Yield: 44.8%, light yellow solid. Mp: 53−54 °C. ^{1}H NMR (300 MHz, DMSO-d_6) δ: 7.85 (s, 1H), 7.47−7.54 (m, 4H), 7.23−7.30 (m, 6H), 7.00 (s, 1H), 6.01 (s, 1H), 4.33 (t, 2H, J = 6.8 Hz), 3.97 (m, 2H), 3.58 (m, 1H), 2.64 (m, 1H), 1.96 (m, 4H), 0.92 (t, 3H, J = 7.2 Hz). ESI-MS (m/z): 504.29 $[M + H]^+$. HPLC purity: 98.6%.

5-(3-(1H-Imidazol-1-yl)propyl)-4-(4-bromophenyl)-1-isopropyl-3-phenyl-4,5-dihydropyrrolo[3,4-c]pyrazol-6(1H)-one ***(5d)***. Yield: 45.3%, light yellow solid. Mp: 80−81 °C. ^{1}H NMR (500 MHz, DMSO-d_6) δ: 7.65 (s, 1H), 7.47−7.54 (m, 4H), 7.22−7.34 (m, 5H), 7.17 (s, 1H), 6.89 (s, 1H), 5.98 (s, 1H), 4.85 (m, 1H), 3.97 (m, 2H), 3.58 (m, 1H), 2.65 (m, 1H), 1.90 (m, 2H), 1.59 (d, 6H, J = 6.6 Hz). ESI-MS (m/z): 504.29 $[M + H]^+$. HPLC purity: 95.6%.

5-(3-(1H-Imidazol-1-yl)propyl)-4-(4-bromophenyl)-1-butyl-3-phenyl-4,5-dihydropyrrolo[3,4-c]pyrazol-6(1H)-one ***(5e)***. Yield: 35.4%, light yellow solid. Mp: 50−51 °C.^{1}H NMR (300 MHz, DMSO-d_6) δ: 7.61 (s, 1H), 7.51−7.59 (m, 4H), 7.23−7.37 (m, 5H), 7.15 (s, 1H), 6.87 (s, 1H), 6.00 (s, 1H), 4.36 (t, 2H, J = 7.1 Hz), 3.95 (m, 2H), 3.57 (m, 1H), 2.66 (m, 1H), 1.90 (m, 4H), 1.35 (m, 2H), 0.93 (t, 3H, J = 7.5 Hz). ESI-MS (m/z): 518.27 $[M + H]^+$. HPLC purity: 95.5%.

5-(3-(1H-Imidazol-1-yl)propyl)-4-(4-bromophenyl)-1-isobutyl-3-phenyl-4,5-dihydropyrrolo[3,4-c]pyrazol-6(1H)-one ***(5f)***. Yield: 38.0%, white solid. Mp: 75−76 °C. ^{1}H NMR (300 MHz, DMSO-d_6) δ: 7.59 (s, 1H), 7.47−7.55 (m, 4H), 7.21−7.28 (m, 5H), 7.13 (s, 1H), 6.86 (s, 1H), 6.00 (s, 1H), 4.12 (d, 2H, J = 6.6 Hz), 3.93 (m, 2H), 3.57 (m, 1H), 2.65 (m, 1H), 2.34 (m, 1H), 1.88 (m, 2H), 0.83 (d, 6H, J = 6.3 Hz). ESI-MS (m/z): 518.28 $[M + H]^+$. HPLC purity: 95.1%.

5-(3-(1H-Imidazol-1-yl)propyl)-4-(4-bromophenyl)-1-(tert-butyl)-3-phenyl-4,5-dihydropyrrolo[3,4-c]pyrazol-6(1H)-one ***(5g)***. Yield: 24.1%, light yellow solid. Mp: 85−86 °C. ^{1}H NMR (300 MHz, DMSO-d_6) δ: 7.72 (s, 1H), 7.48−7.53 (m, 4H), 7.20−7.30 (m, 6H), 6.93 (s, 1H), 5.93 (s, 1H), 3.95 (m, 2H), 3.60 (m, 1H), 2.66 (m, 1H), 1.93 (m, 2H), 1.73 (s, 9H). ESI-MS (m/z): 518.27 $[M + H]^+$. HPLC purity: 98.3%.

5-(3-(1H-Imidazol-1-yl)propyl)-1-allyl-4-(4-bromophenyl)-3-phenyl-4,5-dihydropyrrolo[3,4-c]pyrazol-6(1H)-one ***(5h)***. Yield: 45.2%, yellow oil. ^{1}H NMR (300 MHz, DMSO-d_6) δ: 7.59 (s, 1H), 7.47−7.54 (m, 4H), 7.21−7.35 (m, 5H), 7.14 (s, 1H), 6.86 (s, 1H), 6.19 (m, 1H), 6.09 (s, 1H), 5.75 (m, 1H), 5.27 (m, 1H), 4.97 (d, 2H, J = 4.5 Hz), 3.93 (m, 2H), 3.56 (m, 1H), 2.64 (m, 1H), 1.88 (m, 2H). ESI-MS (m/z): 502.23 $[M + H]^+$. HPLC purity: 96.0%.

5-(3-(1H-Imidazol-1-yl)propyl)-4-(4-bromophenyl)-3-phenyl-1-(prop-2-yn-1-yl)-4,5-dihydropyrrolo[3,4-c]pyrazol-6(1H)-one ***(5i)***. Yield: 27.7%, yellow solid. Mp: 89−91 °C. ^{1}H NMR (300 MHz, DMSO-d_6) δ: 7.61 (s, 1H), 7.49−7.55 (m, 4H), 7.24−7.32 (m, 5H), 7.15 (s, 1H), 6.87 (s, 1H), 6.05 (s, 1H), 5.21 (s, 1H), 3.96 (m, 2H), 3.61 (m, 2H), 2.65 (m, 1H), 1.91 (m, 2H). ESI-MS (m/z): 500.22 $[M + H]^+$. HPLC purity: 97.0%.

5-(3-(1H-Imidazol-1-yl)propyl)-4-(4-bromophenyl)-1-pentyl-3-phenyl-4,5-dihydropyrrolo[3,4-c]pyrazol-6(1H)-one ***(5j)***. Yield: 26.1%, light yellow solid. Mp: 85−87 °C. ^{1}H NMR (300 MHz, DMSO-d_6) δ: 7.60 (s, 1H), 7.48−7.54 (m, 4H), 7.22−7.30 (m, 5H), 7.14 (s, 1H), 6.86 (s, 1H), 5.99 (s, 1H), 4.34 (t, 2H, J = 6.9 Hz), 3.95 (m, 2H), 3.57 (m, 1H), 2.67 (m, 1H), 1.93 (m, 4H), 1.30 (m, 4H), 0.83 (t, 3H, J = 6.6 Hz). ^{13}C NMR (75 MHz, DMSO-d_6) δ: 157.92, 142.37, 140.28, 137.27, 135.30, 131.99, 131.45, 130.21, 129.45, 128.58, 128.36, 127.95, 125.67, 121.94, 119.18, 57.82, 49.92, 43.52, 37.55, 29.41, 29.24, 28.08, 21.55, 13.82. ESI-MS (m/z): 532.33 $[M + H]^+$. HPLC purity: 96.6%.

5-(3-(1H-Imidazol-1-yl)propyl)-4-(4-bromophenyl)-1-hexyl-3-phenyl-4,5-dihydropyrrolo[3,4-c]pyrazol-6(1H)-one ***(5k)***. Yield: 31.2%, white solid. Mp: 54−55 °C. ^{1}H NMR (300 MHz, DMSO-d_6) δ: 7.61 (s, 1H), 7.47−7.54 (m, 4H), 7.21−7.28 (m, 5H), 7.15 (s, 1H), 6.87 (s, 1H), 6.00 (s, 1H), 4.36 (t, 2H, J = 6.3 Hz), 3.93 (m, 2H), 3.58 (m, 1H), 2.71 (m, 1H), 1.92 (m, 4H), 1.28 (m, 4H), 0.83 (t, 3H, J = 6.6 Hz). ESI-MS (m/z): 546.29 $[M + H]^+$. HPLC purity: 98.2%.

dx.doi.org/10.1021/jm401800k | J. Med. Chem. 2014, 57, 567−577

5-(3-(1H-Imidazol-1-yl)propyl)-4-(4-bromophenyl)-1-heptyl-3-phenyl-4,5-dihydropyrrolo[3,4-c]pyrazol-6(1H)-one ***(5l)***. Yield: 35.7%, yellow oil. ^{1}H NMR (300 MHz, DMSO-d_6) δ: 7.60 (s, 1H), 7.48−7.54 (m, 4H), 7.21−7.28 (m, 5H), 7.15 (s, 1H), 6.87 (s, 1H), 6.00 (s, 1H), 4.36 (t, 2H, J = 6.3 Hz), 3.93 (m, 2H), 3.58 (m, 1H), 2.71 (m, 1H), 1.92 (m, 4H), 1.28 (m, 6H), 0.82 (t, 3H, J = 6.6 Hz). ESI-MS (m/z): 560.41 [M + H]$^+$. HPLC purity: 95.1%.

5-(3-(1H-Imidazol-1-yl)propyl)-4-(4-bromophenyl)-1-octyl-3-phenyl-4,5-dihydropyrrolo[3,4-c]pyrazol-6(1H)-one ***(5m)***. Yield: 33.6%, yellow oil. ^{1}H NMR (300 MHz, DMSO-d_6) δ: 7.59 (s, 1H), 7.50−7.53 (m, 4H), 7.21−7.29 (m, 5H), 7.14 (s, 1H), 6.86 (s, 1H), 6.00 (s, 1H), 4.33 (t, 2H, J = 6.8 Hz), 3.93 (m, 2H), 3.45 (m, 1H), 2.66 (m, 1H), 1.90 (m, 2H), 1.20 (m, 12H), 0.79 (t, 3H, J = 7.5 Hz). ESI-MS (m/z): 574.40 [M + H]$^+$. HPLC purity: 95.2%.

5-(3-(1H-Imidazol-1-yl)propyl)-4-(4-bromophenyl)-1-cyclobutyl-3-phenyl-4,5-dihydropyrrolo[3,4-c]pyrazol-6(1H)-one ***(5n)***. Yield: 29.2%, yellow solid. Mp: 87−89 °C. ^{1}H NMR (300 MHz, DMSO-d_6) δ: 7.64 (s, 1H), 7.49−7.55 (m, 4H), 7.20−7.30 (m, 5H), 7.17 (s, 1H), 6.89 (s, 1H), 5.99 (s, 1H), 5.13 (m, 1H), 3.99 (m, 2H), 3.59 (m, 1H), 2.80 (m, 4H), 2.65 (m, 1H), 1.88 (m, 4H). ESI-MS (m/z): 516.26 [M + H]$^+$. HPLC purity: 95.6%.

5-(3-(1H-Imidazol-1-yl)propyl)-4-(4-bromophenyl)-1-cyclopentyl-3-phenyl-4,5-dihydropyrrolo[3,4-c]pyrazol-6(1H)-one ***(5o)***. Yield: 41.6%, white solid. Mp: 80−83 °C. ^{1}H NMR (300 MHz, DMSO-d_6) δ: 7.75 (s, 1H), 7.47−7.54 (m, 4H), 7.20−7.30 (m, 6H), 6.93 (s, 1H), 5.98 (s, 1H), 5.07 (m, 1H), 3.96 (m, 2H), 3.58 (m, 1H), 2.65 (m, 1H), 2.18 (m, 4H), 1.92 (m, 4H), 1.69 (m, 2H). ESI-MS (m/z): 530.50 [M + H]$^+$. HPLC purity: 96.7%.

5-(3-(1H-Imidazol-1-yl)propyl)-4-(4-bromophenyl)-1-cyclohexyl-3-phenyl-4,5-dihydropyrrolo[3,4-c]pyrazol-6(1H)-one ***(5p)***. Yield: 23.5%, yellow oil. ^{1}H NMR (300 MHz, DMSO-d_6) δ: 7.60 (s, 1H), 7.47−7.54 (m, 4H), 7.22−7.30 (m, 5H), 7.15 (s, 1H), 6.86 (s, 1H), 6.00 (s, 1H), 3.93 (m, 2H), 3.57 (m, 1H), 2.66 (m, 2H), 1.99 (m, 6H), 1.28 (m, 6H). ESI-MS (m/z): 544.26 [M + H]$^+$. HPLC purity: 95.6%.

5-(3-(1H-Imidazol-1-yl)propyl)-1-benzyl-4-(4-bromophenyl)-3-phenyl-4,5-dihydropyrrolo[3,4-c]pyrazol-6(1H)-one ***(5q)***. Yield: 55.1%, white solid. Mp: 78−79 °C. ^{1}H NMR (300 MHz, DMSO-d_6) δ: 7.61 (s, 1H), 7.51−7.59 (m, 4H), 7.23−7.36 (m, 10H), 7.15 (s, 1H), 6.87 (s, 1H), 6.02 (s, 1H), 5.59 (s, 2H), 3.98 (m, 2H), 3.59 (m, 1H), 2.63 (m, 1H), 1.88 (m, 2H). ^{13}C NMR (75 MHz, DMSO-d_6) δ: 157.89, 143.06, 140.37, 137.27, 136.68, 135.08, 132.03, 131.21, 130.25, 129.84, 128.77, 128.62, 128.14, 127.99, 127.88, 125.76, 121.97, 119.21, 57.85, 53.31, 43.52, 37.62, 29.40. ESI-MS (m/z): 552.15 [M + H]$^+$. HPLC purity: 95.8%.

5-(3-(1H-Imidazol-1-yl)propyl)-4-(4-bromophenyl)-1-(2-fluorobenzyl)-3-phenyl-4,5-dihydropyrrolo[3,4-c]pyrazol-6(1H)-one ***(5r)***. Yield: 53.5%, yellow solid. Mp: 98−102 °C. ^{1}H NMR (300 MHz, DMSO-d_6) δ: 7.64 (s, 1H), 7.41−7.54 (m, 5H), 7.17−7.31 (m, 8H), 7.15 (m, 2H), 6.88 (s, 1H), 6.02 (s, 1H), 5.57 (s, 2H), 3.94 (m, 2H), 3.62 (m, 1H), 2.69 (m, 1H), 1.89 (m, 2H). ESI-MS (m/z): 570.36 [M + H]$^+$. HPLC purity: 95.9%.

5-(3-(1H-Imidazol-1-yl)propyl)-4-(4-bromophenyl)-1-(4-fluorobenzyl)-3-phenyl-4,5-dihydropyrrolo[3,4-c]pyrazol-6(1H)-one ***(5s)***. Yield: 64.3%, yellow solid. Mp: 113−115 °C. ^{1}H NMR (300 MHz, DMSO-d_6) δ: 7.62 (s, 1H), 7.47−7.56 (m, 6H), 7.20−7.31 (m, 7H), 7.15 (s, 1H), 6.88 (s, 1H), 6.02 (s, 1H), 5.54 (s, 2H), 3.97 (m, 2H), 3.60 (m, 1H), 2.67 (m, 1H), 1.90 (m, 2H). ^{13}C NMR (75 MHz, DMSO-d_6) δ: 164.26, 161.03, 158.68, 143.94, 141.12, 138.06, 135.86, 133.72, 132.93, 131.99, 131.06, 130.91, 130.73, 129.42, 129.06, 128.98, 126.58, 122.79, 120.04, 116.55, 116.27, 58.70, 53.37, 44.36, 38.45, 30.18. ESI-MS (m/z): 570.30 [M + H]$^+$. HPLC purity: 98.4%.

5-(3-(1H-Imidazol-1-yl)propyl)-4-(4-bromophenyl)-3-phenyl-1-(2-((tetrahydro-2H-pyran-2-yl)oxy)ethyl)-4,5-dihydropyrrolo[3,4-c]pyrazol-6(1H)-one ***(5t)***. Yield: 31.4%, light yellow solid. Mp: 52−53 °C. ^{1}H NMR (300 MHz, DMSO-d_6) δ: 7.60 (s, 1H), 7.49−7.56 (m, 4H), 7.22−7.29 (m, 5H), 7.14 (s, 1H), 6.87 (s, 1H), 6.03 (s, 1H), 4.53−4.61 (m, 3H), 4.03 (m, 1H), 3.97 (m, 3H), 3.62 (m, 2H), 3.43 (m, 1H), 2.71 (m, 1H), 1.91 (m, 2H), 1.66 (m, 2H), 1.41 (m, 6H). ESI-MS (m/z): 590.21 [M + H]$^+$. HPLC purity: 95.9%.

5-(3-(1H-Imidazol-1-yl)propyl)-4-(4-bromophenyl)-1-(2-hydroxyethyl)-3-phenyl-4,5-dihydropyrrolo[3,4-c]pyrazol-6(1H)-one ***(5u)***. Yield: 25.1%, white solid. Mp: 74−75 °C. ^{1}H NMR (300 MHz, DMSO-d_6) δ: 7.61 (s, 1H), 7.47−7.54 (m, 4H), 7.19−7.30 (m, 5H), 7.15 (s, 1H), 6.86 (s, 1H), 5.98 (s, 1H), 5.00 (br, 1H), 4.40 (t, 2H, J = 5.6 Hz), 3.96 (m, 4H), 3.61 (m, 1H), 2.66 (m, 1H), 1.91 (m, 2H). ^{13}C NMR (75 MHz, DMSO-d_6) δ: 157.96, 142.44, 140.82, 137.29, 135.37, 131.94, 131.50, 130.30, 129.48, 128.58, 128.33, 127.94, 125.67, 121.91, 119.19, 59.68, 57.78, 52.88, 43.56, 37.53, 29.38. ESI-MS (m/z): 506.48 [M + H]$^+$. HPLC purity: 96.0%.

Ethyl 2-(5-(3-(1H-Imidazol-1-yl)propyl)-4-(4-bromophenyl)-6-oxo-3-phenyl-5,6-dihydropyrrolo[3,4-c]pyrazol-1(4H)-yl)acetate ***(5v)***. Yield: 35.3%, yellow solid. Mp: 128−130 °C. ^{1}H NMR (300 MHz, DMSO-d_6) δ: 7.58 (s, 1H), 7.48−7.56 (m, 4H), 7.21−7.32 (m, 5H), 7.13 (s, 1H), 6.86 (s, 1H), 6.07 (s, 1H), 5.26 (s, 2H), 4.24 (m, 2H), 3.97 (m, 2H), 3.59 (m, 1H), 2.66 (m, 1H), 1.88 (m, 2H), 1.22 (t, 3H, J = 7.1 Hz). ESI-MS (m/z): 548.24 [M + H]$^+$. HPLC purity: 96.6%.

Ethyl 3-(5-(3-(1H-Imidazol-1-yl)propyl)-4-(4-bromophenyl)-6-oxo-3-phenyl-5,6-dihydropyrrolo[3,4-c]pyrazol-1(4H)-yl)-propanoate ***(5w)***. Yield: 39.8%, light yellow oil. ^{1}H NMR (300 MHz, DMSO-d_6) δ: 7.59 (s, 1H), 7.46−7.54 (m, 4H), 7.22−7.30 (m, 5H), 7.13 (s, 1H), 6.86 (s, 1H), 6.00 (s, 1H), 4.61 (t, 2H, J = 6.8 Hz), 4.06 (m, 2H), 3.96 (m, 2H), 3.61 (m, 1H), 3.09 (t, 2H, J = 6.6 Hz), 2.66 (m, 1H), 1.88 (m, 2H), 1.13 (t, 3H, J = 7.1 Hz). ESI-MS (m/z): 562.25 [M + H]$^+$. HPLC purity: 96.1%.

Ethyl 4-(5-(3-(1H-Imidazol-1-yl)propyl)-4-(4-bromophenyl)-6-oxo-3-phenyl-5,6-dihydropyrrolo[3,4-c]pyrazol-1(4H)-yl)butanoate ***(5x)***. Yield: 45.0%, light yellow oil. ^{1}H NMR (300 MHz, DMSO-d_6) δ: 7.59 (s, 1H), 7.48−7.54 (m, 4H), 7.22−7.30 (m, 5H), 7.13 (s, 1H), 6.86 (s, 1H), 5.98 (s, 1H), 4.41 (t, 2H, J = 6.6 Hz), 4.00 (m, 4H), 3.53 (m, 1H), 2.65 (m, 1H), 2.41 (m, 2H), 2.21 (m, 2H), 1.88 (m, 2H), 1.11 (t, 3H, J = 7.2 Hz). ESI-MS (m/z): 576.65 [M + H]$^+$. HPLC purity: 97.3%.

Fluorescence Polarization Binding Assay.[19,42,43] Briefly, the fluorescence polarization experiments were read on Biotek Synergy H2 with the 485 nm excitation and 535 nm emission filters. The fluorescence intensities parallel ($Int_{parallel}$) and perpendicular ($Int_{perpedicular}$) to the plane of excitation were measured in black, 96-well plates with nonbinding surface (Corning #3993) at room temperature. The background fluorescence intensities of blank samples containing the reference buffer were subtracted, and the steady-state fluorescence polarization was calculated using the equation $P = 1000 \times (Int_{parallel} - GInt_{perpedicular})/(Int_{parallel} + GInt_{perpedicular})$. The correction factor G (G = 0.998 determined empirically) was introduced to eliminate differences in the transmission of vertically and horizontally polarized light. All fluorescence polarization values were expressed in millipolarization units (mP). The dose-dependent binding experiments were carried out with serial dilution in DMSO of compounds. A 5 μL sample of the test sample, preincubated (for 30 min) MDM2 binding domain (1−118) (10 nM), and PMDM6-F peptide (Anaspec) (10 nM) in assay buffer (100 mM potassium phosphate, pH 7.5; 100 μg/mL bovine gamma globulin; 0.02% sodium azide) were added to microplates to produce a final volume of 115 μL. For each assay, the controls contained the MDM2 binding domain and PMDM6-F. Plates were read at 1 h after mixing all assay components. Binding constant (K_i) was determined by fitting inhibition curves using GraphPad Prism software. Nutlin-3 (Sigma-Aldrich) was used as reference compound for validating the assay in each plate.

In Vitro Antiproliferative Assay. The cellular growth inhibitory activity was determined using two human osteosarcoma cell lines [U-2 OS (wild type p53) and Saos-2 (p53 null)] and two human lung cancer cell lines [A549 (wild-type p53) and NCI-H1299 (p53 null)]. An amount of (5−6) × 10^4 cells per well was transferred to 96-well plates. After culturing for 24 h, the test compounds were added to triplicate wells at different concentrations and 0.1% DMSO for control. After 72 h of incubation, 20 μL of MTT [3-(4,5-dimethylthiazol-2-yl)-2,5-diphenyltetrazolium bromide] solution (5 mg/mL) was added to each well, and after the samples were shaken for 1 min, the plate was incubated further for 4 h at 37 °C. Compounds were dissolved in 100 μL of DMSO. The absorbance (OD) was quantitated with the microplates using Biotek Synergy H2 at 570 nm. Wells containing no

dx.doi.org/10.1021/jm401800k | J. Med. Chem. 2014, 57, 567−577

drugs were used as blanks. The concentration of the compounds that inhibited cell growth by 50% (IC_{50}) was calculated. Nutlin-3 (Sigma-Aldrich) was used as a reference compound for validating the assay in each plate.

Western Blotting Assay. A549 cancer cell lines harboring wild-type p53 were grown in the recommended media supplemented with 10% FBS (Invitrogen) in a humidified environment with 5% CO_2. After 4 h treatment with various concentrations of the compounds, cells were lysed, and the protein extract was denatured and run on 5% trisglycine polyacrylamide gels (Invitrogen). Gels were electroblotted onto nitrocellulose membranes, and Western detection was carried out using 5% milk buffer (5% nonfat dry milk in TBS/0.1% Tween-20) throughout. Proteins were detected by ECL chemiluminescence reagents (Pierce, #32209) using antibodies specific for human p53 (Calbiochem, #OP43T), MDM2 (Millipore, #07-575), NF-κB p65 (D14E12) rabbit mAb (CST, # 8242S), NF-κB (p105/p50) (NFKB1) antibody (Epitomic, #1559-1), IKKα (abcam, #1615-1), IKKβ (IKBKB) antibody (abcam, #3902-1), IKKγ (DA10-12) mouse mAb (CST, #2695S), phospho-IKKα/β (Ser176/180) (16A6) rabbit mAb (CST, #2697S), phospho-IKKγ (Ser376) antibody (CST, #2689S), phospho-IκBα (Ser32) (14D4) rabbit mAb (CST, #2859S), IκBα (44D4) rabbit mAb (CST, #4812S), GAPDH antibody (multiscience, #mab5465), and histone 3 (D1H2) XP rabbit mAb (CST, #4499P).

Indirect Immunofluorescence Assay.[44] The nuclear translocation of NF-κB p65 was examined by an indirect immunofluorescence assay. Briefly, A549 cells were cultured in six-well plates (2×10^5 cells per well) for 24 h and then pretreated with compounds **5q** or **5s** at 10 μM for 4 h. The cells were then washed and fixed with anhydrous methanol for 15 min at room temperature, permeabilized with 0.1% Triton X-100 for 15 min, and blocked with 1% BSA for 10 min at room temperature. Next, cells were incubated with primary anti-NF-κB p65 antibody in PBS overnight at 4 °C, followed by Cy3-conjugated secondary antibodies. After being washed with PBS three times, cells were incubated in 10 μM Hochest 33342 for 15 min in the dark. The fluorescence of the p65 protein and nucleus were red and blue, respectively, and live cell imaging was simultaneously accomplished using a microscopy system (Olympus BX-51, Toyko, Japan).

Cell-Free Kinase Assay. Compound **5s** was evaluated by Cerep Kinase Profiler service (Shanghai, P. R. China) for its inhibitory activities against seven related kinases of the NF-κB pathway, including IKKα, IKKβ, IKKε, CHK1, Akt1, Akt2, and Akt3. All the experiments were carried out as described in the literature.[45−48]

In Vivo Antiproliferative Assay. The in vivo antitumor activity of compounds **5j**, **5q**, **5s**, and **5u** was evaluated. DOX was used as a reference drug. BALB/C nude male mice (certificate SCXK2003-0003, weighing 18−20 g) were obtained from Shanghai Experimental Animal Center, Chinese Academy of Sciences. A549 cancer cell suspensions were implanted subcutaneously into the right axilla region of the mice. The compounds were solved in normal saline with a drop of hydrochloric acid and administrated by i.g. route. Treatment began when implanted tumors had reached a volume of about 120 mm^3 (after 13 days). The animals were randomized into appropriate groups (six animals per treatment and 10 animals for the control group) and administered by gavage once daily for 14 consecutive days from day 13 after implantation of the cells. Tumor volumes (TV) were monitored by caliper measurement of the length and width and then calculated using the formula of $TV = {}^1/_2ab^2$, where a is the tumor length and b is the width. Tumor volumes and body weights were monitored every 4 days over the course of treatment. Mice were sacrificed on day 29 after implantation of cells, and tumors were removed and recorded for analysis. Tumor volume inhibition was determined by the formula $1 - RTV_{tumor}/RTV_{control} \times 100\%$, where RTV is the relative tumor volume to that of day 13. DOX (10 mg/kg, Pfizer Italia S.r.l) was administered intravenously once on day 13 after implantation.

Pharmacokinetic Studies in Rats. Pharmacokinetic studies of compound **5q** were performed in male Sprague−Dawley rats (Certificate SCXK2010-0049, weighing 200−250 g, Shanghai Sippr-BK Laboratory Animals). For HPLC analysis, a stock solution of compound **5q** was prepared by dissolving it in 70% methanol to yield a final concentration of 500 μg/mL. This solution was then diluted using 70% methanol to get a series of working solutions of 20, 10, 2, 1, 0.2, 0.1, and 0.02 μg/mL. Seven calibration standard solutions containing 1000, 500, 100, 50, 10, 5, and 1 ng/mL were obtained by adding 1.5 μL of working solution prepared above into seven Eppendorff tubes containing 30 μL of blank plasma. Samples for quality control were prepared as well to get the final concentration of 800, 80, and 8 ng/mL. Diphenhydramine (100 ng/mL) was used as the internal standard. Compound **5q** was administrated intravenously (i.v.) and intragastrically (i.g.) in two groups (four male rats per group). In the i.v. group, blood samples were collected from orbit at predose and 0.05, 0.133, 0.25, 0.5, 1, 2, 4, 6, 8, 10, and 12 h. In the i.g. group, blood samples were collected from orbit at predose and 0.083, 0.5, 1, 1.5, 2, 3, 4, 6, 8, 10, 12, and 24 h. Plasma samples were obtained and stored at −40 °C until bioanalysis. Plasma samples were processed by protein precipitation. Plasma samples (30 μL) were transferred to Eppendorff tube, then 1.5 μL of 70% methanol, 30 μL of diphenhydramine (100 ng/mL), and 90 μL of methanol were added to it. After vortexing and centrifuging for 4 min at 13 000 rpm, samples were filtered using 0.22-μm Millipore membranes, then 2 μL was used for injection. Aqueous ammonium formate (10 mM)/CH_3CN (10:90) was used as the mobile phase with a flow rate of 0.3 mL/min on a Kromasil C_{18} (150 × 2.1 mm) on an Ultimate 3000 liquid chromatograph (Dionex) for this study. Mass spectrometric analysis was performed using a 4000 Q-Trap instrument from AB Inc. with an ESI interface. Data were processed using DAS 2.0 software. Pharmacokinetic data analysis was performed using noncompartmental analysis. The absolute bioavailability (F_{ab}) was determined by the formula $F_{ab} = AUC_{i.g.} \times dose_{i.v.}/AUC_{i.v.} \times dose_{i.g.}$. Normal saline with Tween-80 (3%) and CMCNa (0.5%) was used for the i.g. route. Normal saline with DMSO (5%) and castor oil (5%) was used for the i.v. route in the PK study.

AUTHOR INFORMATION

Corresponding Authors

*Z.M.: phone/fax, 86-21-81871241; e-mail: miaozhenyuan@hotmail.com.

*C.S.: phone/fax, 86-21-81871239; e-mail: shengcq@hotmail.com.

*W.Z.: phone/fax, 86-21-81871243; e-mail: zhangwnk@hotmail.com.

Notes

The authors declare no competing financial interest.

ACKNOWLEDGMENTS

We thank the National Natural Science Foundation of China (grant 81373331, 81222044), the 863 Hi-Tech Program of China (grant 2012AA020302), the National Basic Research Program of China (grant 2014CB541800), Shanghai Rising-Star Program (grant 12QH1402600), Shanghai Municipal Health Bureau (grant XYQ2011038), and Second Military Medical University (Ph.DInnovation Fellowship) for financial support. We are grateful to China Scholarship Council's Abroad Training Plan for Ph.D candidates. We also greatly appreciate the valuable suggestions of Prof. Ding Jing from Eastern Hepatobiliary Surgery Hospital.

ABBREVIATIONS USED

NF-κB, nuclear factor kappa B; MDM2, murine double minute 2; FP, fluorescence polarization; SAR, structure−activity relationship; THP, tetrahydropyranyl; IC_{50}, 50% inhibitory concentration; DOX, doxorubicin; FBS, fetal bovine serum; TV, tumor volume; RTV, relative tumor volume; IκBα, nuclear factor of kappa light polypeptide gene enhancer in B-cells inhibitor alpha; F_{ab}, absolute bioavailability.

REFERENCES

(1) Vogelstein, B.; Lane, D.; Levine, A. J. Surfing the p53 network. *Nature* **2000**, *408*, 307−310.

(2) Vousden, K. H.; Lane, D. P. p53 in health and disease. *Nat. Rev. Mol. Cell. Biol.* **2007**, *8*, 275−283.

(3) Levine, A. J. p53, the cellular gatekeeper for growth and division. *Cell* **1997**, *88*, 323−31.

(4) Joerger, A. C.; Fersht, A. R. Structural biology of the tumor suppressor p53 and cancer-associated mutants. *Adv. Cancer Res.* **2007**, *97*, 1−23.

(5) Joerger, A. C.; Fersht, A. R. Structural biology of the tumor suppressor p53. *Annu. Rev. Biochem.* **2008**, *77*, 557−582.

(6) Toledo, F.; Wahl, G. M. Regulating the p53 pathway: In vitro hypotheses, in vivo veritas. *Nat Rev Cancer* **2006**, *6*, 909−923.

(7) Vousden, K. H.; Prives, C. Blinded by the light: The growing complexity of p53. *Cell* **2009**, *137*, 413−431.

(8) Boeckler, F. M.; Joerger, A. C.; Jaggi, G.; Rutherford, T. J.; Veprintsev, D. B.; Fersht, A. R. Targeted rescue of a destabilized mutant of p53 by an in silico screened drug. *Proc. Natl. Acad. Sci. U. S. A.* **2008**, *105*, 10360−10365.

(9) Brown, C. J.; Lain, S.; Verma, C. S.; Fersht, A. R.; Lane, D. P. Awakening guardian angels: Drugging the p53 pathway. *Nat. Rev. Cancer* **2009**, *9*, 862−873.

(10) Popowicz, G. M.; Czarna, A.; Holak, T. A. Structure of the human Mdmx protein bound to the p53 tumor suppressor transactivation domain. *Cell Cycle* **2008**, *7*, 2441−2443.

(11) Joerger, A. C.; Fersht, A. R. The tumor suppressor p53: From structures to drug discovery. *Cold Spring Harbor Perspect. Biol.* **2010**, *2*, a000919.

(12) Millard, M.; Pathania, D.; Grande, F.; Xu, S.; Neamati, N. Small-molecule inhibitors of p53−MDM2 interaction: The 2006−2010 update. *Curr. Pharm. Des.* **2011**, *17*, 536−559.

(13) Vassilev, L. T.; Vu, B. T.; Graves, B.; Carvajal, D.; Podlaski, F.; Filipovic, Z.; Kong, N.; Kammlott, U.; Lukacs, C.; Klein, C.; Fotouhi, N.; Liu, E. A. In vivo activation of the p53 pathway by small-molecule antagonists of MDM2. *Science* **2004**, *303*, 844−848.

(14) Wade, M.; Wang, Y. V.; Wahl, G. M. The p53 orchestra: Mdm2 and Mdmx set the tone. *Trends Cell. Biol.* **2010**, *20*, 299−309.

(15) Grasberger, B. L.; Lu, T.; Schubert, C.; Parks, D. J.; Carver, T. E.; Koblish, H. K.; Cummings, M. D.; LaFrance, L. V.; Milkiewicz, K. L.; Calvo, R. R.; Maguire, D.; Lattanze, J.; Franks, C. F.; Zhao, S.; Ramachandren, K.; Bylebyl, G. R.; Zhang, M.; Manthey, C. L.; Petrella, E. C.; Pantoliano, M. W.; Deckman, I. C.; Spurlino, J. C.; Maroney, A. C.; Tomczuk, B. E.; Molloy, C. J.; Bone, R. F. Discovery and cocrystal structure of benzodiazepinedione HDM2 antagonists that activate p53 in cells. *J. Med. Chem.* **2005**, *48*, 909−912.

(16) Ding, K.; Lu, Y.; Nikolovska-Coleska, Z.; Qiu, S.; Ding, Y.; Gao, W.; Stuckey, J.; Krajewski, K.; Roller, P. P.; Tomita, Y.; Parrish, D. A.; Deschamps, J. R.; Wang, S. Structure-based design of potent non-peptide MDM2 inhibitors. *J. Am. Chem. Soc.* **2005**, *127*, 10130−10131.

(17) Wang, S. M.; Ding, K.; Lu, Y. P.; Nikolovska-Coleska, Z.; Qiu, S.; Kumar, S.; Roller, P. P.; Tomita, Y.; Krajewski, K.; Deschamps, J. R. Structure-based design of potent, non-peptide small-molecule inhibitors of the MDM2-p53 interaction starting from an inactive lead. *Abstr. Pap. Am. Chem. Soc.* **2005**, *230*, U2700−U2700.

(18) Rew, Y.; Sun, D.; Gonzalez-Lopez De Turiso, F.; Bartberger, M. D.; Beck, H. P.; Canon, J.; Chen, A.; Chow, D.; Deignan, J.; Fox, B. M.; Gustin, D.; Huang, X.; Jiang, M.; Jiao, X.; Jin, L.; Kayser, F.; Kopecky, D. J.; Li, Y.; Lo, M. C.; Long, A. M.; Michelsen, K.; Oliner, J. D.; Osgood, T.; Ragains, M.; Saiki, A. Y.; Schneider, S.; Toteva, M.; Yakowec, P.; Yan, X.; Ye, Q.; Yu, D.; Zhao, X.; Zhou, J.; Medina, J. C.; Olson, S. H. Structure-based design of novel inhibitors of the MDM2−p53 interaction. *J. Med. Chem.* **2012**, *55*, 4936−4954.

(19) Zhuang, C.; Miao, Z.; Zhu, L.; Dong, G.; Guo, Z.; Wang, S.; Zhang, Y.; Wu, Y.; Yao, J.; Sheng, C.; Zhang, W. Discovery, synthesis, and biological evaluation of orally active pyrrolidone derivatives as novel inhibitors of p53−MDM2 protein−protein interaction. *J. Med. Chem.* **2012**, *55*, 9630−9642.

(20) Sen, R.; Baltimore, D. Inducibility of kappa immunoglobulin enhancer-binding protein Nf-kappa B by a posttranslational mechanism. *Cell* **1986**, *47*, 921−928.

(21) Chen, F.; Castranova, V.; Shi, X. L. New insights into the role of nuclear factor-kappa B in cell growth regulation. *Am. J. Pathol.* **2001**, *159*, 387−397.

(22) Collins, T.; Read, M. A.; Neish, A. S.; Whitley, M. Z.; Thanos, D.; Maniatis, T. Transcriptional Regulation of Endothelial-Cell Adhesion Molecules—Nf-kappa-B and cytokine-inducible enhancers. *Faseb J* **1995**, *9*, 899−909.

(23) Gilmore, T. D.; Herscovitch, M. Inhibitors of NF-kappa B signaling: 785 and counting. *Oncogene* **2006**, *25*, 6887−6899.

(24) Shishodia, S.; Aggarwal, B. B. Nuclear factor-kappaB activation: A question of life or death. *J. Biochem. Mol. Biol.* **2002**, *35*, 28−40.

(25) Pahl, H. L. Activators and target genes of Rel/NF-kappaB transcription factors. *Oncogene* **1999**, *18*, 6853−6866.

(26) Gurova, K. V.; Hill, J. E.; Guo, C. H.; Prokvolit, A.; Burdelya, L. G.; Samoylova, E.; Khodyakova, A. V.; Ganapathi, R.; Ganapathi, M.; Tararova, N. D.; Bosykh, D.; Lvovskiy, D.; Webb, T. R.; Stark, G. R.; Gudkov, A. V. Small molecules that reactivate p53 in renal cell carcinoma reveal a NF-kappa B-dependent mechanism of p53 suppression in tumors. *Proc. Natl. Acad. Sci. U. S. A.* **2005**, *102*, 17448−17453.

(27) Tergaonkar, V.; Pando, M.; Vafa, O.; Wahl, G.; Verma, I. P53 stabilization is decreased upon NF kappa B activation: A role for NF kappa B in acquisition of resistance to chemotherapy. *Cancer Cell* **2002**, *1*, 493−503.

(28) Dey, A.; Tergaonkar, V.; Lane, D. P. Double-edged swords as cancer therapeutics: Simultaneously targeting p53 and NF-kappaB pathways. *Nat. Rev. Drug Discovery* **2008**, *7*, 1031−1040.

(29) Zimmermann, G. R.; Lehar, J.; Keith, C. T. Multi-target therapeutics: When the whole is greater than the sum of the parts. *Drug Discovery Today* **2007**, *12*, 34−42.

(30) Brasca, M. G.; Albanese, C.; Alzani, R.; Amici, R.; Avanzi, N.; Ballinari, D.; Bischoff, J.; Borghi, D.; Casale, E.; Croci, V.; Fiorentini, F.; Isacchi, A.; Mercurio, C.; Nesi, M.; Orsini, P.; Pastori, W.; Pesenti, E.; Pevarello, P.; Roussel, P.; Varasi, M.; Volpi, D.; Vulpetti, A.; Ciomei, M. Optimization of 6,6-dimethyl pyrrolo[3,4-*c*]pyrazoles: Identification of PHA-793887, a potent CDK inhibitor suitable for intravenous dosing. *Bioorgan Med Chem* **2010**, *18*, 1844−1853.

(31) Chen, H. J.; Liu, Y.; Wang, L. N.; Shen, Q.; Li, J.; Nan, F. J. Discovery and structural optimization of pyrazole derivatives as novel inhibitors of Cdc25B. *Bioorg. Med. Chem. Lett.* **2010**, *20*, 2876−2879.

(32) Fancelli, D.; Berta, D.; Bindi, S.; Cameron, A.; Cappella, P.; Carpinelli, P.; Catana, C.; Forte, B.; Giordano, P.; Giorgini, M. L.; Mantegani, S.; Marsiglio, A.; Meroni, M.; Moll, J.; Pittala, V.; Roletto, F.; Severino, D.; Soncini, C.; Storici, P.; Tonani, R.; Varasi, M.; Vulpetti, A.; Vianello, P. Potent and selective aurora inhibitors identified by the expansion of a novel scaffold for protein kinase inhibition. *J. Med. Chem.* **2005**, *48*, 3080−3084.

(33) Fancelli, D.; Moll, J.; Varasi, M.; Bravo, R.; Artico, R.; Berta, D.; Bindi, S.; Cameron, A.; Candiani, I.; Cappella, P.; Carpinelli, P.; Croci, W.; Forte, B.; Giorgini, M. L.; Klapwijk, J.; Marsiglio, A.; Pesenti, E.; Rocchetti, M.; Roletto, F.; Severino, D.; Soncini, C.; Storici, P.; Tonani, R.; Zugnoni, P.; Vianello, P. 1,4,5,6-tetrahydropyrrolo[3,4-*c*]pyrazoles: Identification of a potent aurora kinase inhibitor with a favorable antitumor kinase inhibition profile. *J. Med. Chem.* **2006**, *49*, 7247−7251.

(34) Grant, S.; Tran, P.; Zhang, Q.; Zou, A. H.; Dinh, D.; Jensen, J.; Zhou, S.; Kang, X. L.; Zachwieja, J.; Lippincott, J.; Liu, K.; Johnson, S. L.; Scales, S.; Yin, C. F.; Nukui, S.; Stoner, C.; Prasanna, G.; Lafontaine, J.; Wells, P.; Li, H. Discovery of a novel class of targeted kinase inhibitors that blocks protein kinase C signaling and ameliorates retinal vascular leakage in a diabetic rat model. *Eur. J. Pharmacol.* **2010**, *627*, 16−25.

(35) Ochiana, S. O.; Pandarinath, V.; Wang, Z. X.; Kapoor, R.; Ondrechen, M. J.; Ruben, L.; Pollastri, M. P. The human Aurora kinase inhibitor danusertib is a lead compound for anti-trypanosomal

drug discovery via target repurposing. *Eur. J. Med. Chem.* **2013**, *62*, 777−784.
(36) Pevarello, P.; Fancelli, D.; Vulpetti, A.; Amici, R.; Villa, M.; Pittala, V.; Vianello, P.; Cameron, A.; Ciomei, M.; Mercurio, C.; Bischoff, J. R.; Roletto, F.; Varasi, M.; Brasca, M. G. 3-Amino-1,4,5,6-tetrahydropyrrolo[3,4-*c*]pyrazoles: A new class of CDK2 inhibitors. *Bioorg. Med. Chem. Lett.* **2006**, *16*, 1084−1090.
(37) Lee, D. H.; Macintyre, J. P.; Taylor, G. R.; Wang, E.; Plante, R. K.; Tam, S. S.; Pope, B. L.; Lau, C. Y. Tepoxalin enhances the activity of an antioxidant, pyrrolidine dithiocarbamate, in attenuating tumor necrosis factor alpha-induced apoptosis in WEHI 164 cells. *J. Pharmacol. Exp. Ther.* **1999**, *289*, 1465−1471.
(38) Lu, Y.; Cederbaum, A. I. CYP2E1 potentiation of LPS and TNF alpha-induced hepatotoxicity by mechanisms involving enhanced oxidative and nitrosative stress, activation of MAP kinases, and mitochondrial dysfunction. *Genes Nutr.* **2010**, *5*, 149−167.
(39) Shishodia, S.; Koul, D.; Aggarwal, B. B. Cyclooxygenase (COX)-2 inhibitor celecoxib abrogates TNF-induced NF-kappa B activation through inhibition of activation of I kappa B alpha kinase and Akt in human non-small cell lung carcinoma: Correlation with suppression of COX-2 synthesis. *J. Immunol.* **2004**, *173*, 2011−2022.
(40) Wu, D.; Xu, C.; Cederbaum, A. Role of nitric oxide and nuclear factor-kappaB in the CYP2E1 potentiation of tumor necrosis factor alpha hepatotoxicity in mice. *Free Radical Biol. Med.* **2009**, *46*, 480−491.
(41) Ghosh, S.; Karin, M. Missing pieces in the NF-kappa B puzzle. *Cell* **2002**, *109*, S81−S96.
(42) Guo, Z.; Zhuang, C.; Zhu, L.; Zhang, Y.; Yao, J.; Dong, G.; Wang, S.; Liu, Y.; Chen, H.; Sheng, C.; Miao, Z.; Zhang, W. Structure−activity relationship and antitumor activity of thio-benzodiazepines as p53−MDM2 protein−protein interaction inhibitors. *Eur. J. Med. Chem.* **2012**, *56*, 10−16.
(43) Zhuang, C.; Miao, Z.; Zhu, L.; Zhang, Y.; Guo, Z.; Yao, J.; Dong, G.; Wang, S.; Liu, Y.; Chen, H.; Sheng, C.; Zhang, W. Synthesis and biological evaluation of thio-benzodiazepines as novel small molecule inhibitors of the p53−MDM2 protein−protein interaction. *Eur. J. Med. Chem.* **2011**, *46*, 5654−5661.
(44) Zhang, T. T.; Sun, L.; Liu, R.; Zhang, D.; Lan, X.; Huang, C.; Xin, W. Y.; Wang, C.; Zhang, D. M.; Du, G. A novel naturally occurring salicylic acid analogue acts as an anti-inflammatory agent by inhibiting nuclear factor-kappaB Activity in RAW264.7 Macrophages. *Mol. Pharmaceutics* **2012**, *9*, 671−677.
(45) Barnett, S. F.; Defeo-Jones, D.; Fu, S.; Hancock, P. J.; Haskell, K. M.; Jones, R. E.; Kahana, J. A.; Kral, A. M.; Leander, K.; Lee, L. L.; Malinowski, J.; McAvoy, E. M.; Nahas, D. D.; Robinson, R. G.; Huber, H. E. Identification and characterization of pleckstrin-homology-domain-dependent and isoenzyme-specific Akt inhibitors. *Biochem. J.* **2005**, *385*, 399−408.
(46) Eddy, S. F.; Guo, S.; Demicco, E. G.; Romieu-Mourez, R.; Landesman-Bollag, E.; Seldin, D. C.; Sonenshein, G. E. Inducible IkappaB kinase/IkappaB kinase epsilon expression is induced by CK2 and promotes aberrant nuclear factor-kappaB activation in breast cancer cells. *Cancer Res.* **2005**, *65*, 11375−11383.
(47) Zhao, B.; Bower, M. J.; McDevitt, P. J.; Zhao, H.; Davis, S. T.; Johanson, K. O.; Green, S. M.; Concha, N. O.; Zhou, B. B. Structural basis for Chk1 inhibition by UCN-01. *J. Biol. Chem.* **2002**, *277*, 46609−46615.
(48) Huynh, Q. K.; Boddupalli, H.; Rouw, S. A.; Koboldt, C. M.; Hall, T.; Sommers, C.; Hauser, S. D.; Pierce, J. L.; Combs, R. G.; Reitz, B. A.; Diaz-Collier, J. A.; Weinberg, R. A.; Hood, B. L.; Kilpatrick, B. F.; Tripp, C. S. Characterization of the recombinant IKK1/IKK2 heterodimer. Mechanisms regulating kinase activity. *J. Biol. Chem.* **2000**, *275*, 25883−25891.